Acta Oceanol. Sin., 2020, Vol. 39, No. 11, P. 33–43
https://doi.org/10.1007/s13131-020-1673-2
http://www.hyxb.org.cn
E-mail: hyxbe@263.net

Effects of tidal currents on winter wind waves in the Qiongzhou Strait: a numerical study

Peng Bai[1, 2], Zheng Ling[2], Cong Liu[3]*, Junshan Wu[4], Lingling Xie[1, 2]

[1] Marine Resources Big Data Center of South China Sea, Southern Marine Science and Engineering Guangdong Laboratory (Zhanjiang), Zhanjiang 524025, China

[2] Guangdong Province Key Laboratory for Coastal Ocean Variation and Disaster Prediction, College of Ocean and Meteorology, Guangdong Ocean University, Zhanjiang 524088, China

[3] Ocean College, Zhejiang University, Zhoushan 316021, China

[4] East China Sea Bureau of Ministry of Natural Resources, Shanghai 200137, China

Received 30 April 2020; accepted 11 June 2020

Abstract

Effects of currents on winter wind waves in the tide-dominated Qiongzhou Strait (QS) were numerically evaluated via employing the coupled ocean-atmosphere-wave-sediment transport (COAWST) modeling system. Validations showed satisfactory model performance in simulating the intense tidal currents in the QS. Different effects of sea level variations and tidal currents on waves were examined under the maximum eastward (METC) and westward (MWTC) tidal currents. In the east entrance area of the QS, the positive sea levels under the MWTC deepened the water depth felt by waves, benefiting the further propagation of wave energy into the inner strait and causing increased wave height. The METC and the MWTC could both enhance the wave height in the east entrance area of the QS, mainly through current-induced convergence and wavenumber shift, respectively. By current-induced refraction, the METC (MWTC) triggered counterclockwise (clockwise) rotation in peak wave directions in the northern part of the QS while clockwise (counterclockwise) rotation in the southern part.

Key words: Qiongzhou Strait, COAWST, significant wave height, peak wave direction

Citation: Bai Peng, Ling Zheng, Liu Cong, Wu Junshan, Xie Lingling. 2020. Effects of tidal currents on winter wind waves in the Qiongzhou Strait: a numerical study. Acta Oceanologica Sinica, 39(11): 33–43, doi: 10.1007/s13131-020-1673-2

1 Introduction

Wave-current interaction represents one of the dominant driving forces in coastal shallow seas, during which process wave dynamics can be considerably modified. When currents are present, the effective wind vector driving the waves is the subtraction of the current vector from the wind vector (Wolf and Prandle, 1999; Fan et al., 2009). Currents can exert refraction, modification of bottom stress, steepening, current-induced breaking, and blocking effects on the waves (Vincent, 1979; Wolf and Prandle, 1999; Ris et al., 1999; Ardhuin et al., 2012). Through Doppler shift, currents change the wave frequency and thereby the phase speed (Tolman, 1990; Wolf and Prandle, 1999). Moreover, the variations of the sea level can also modify wave characteristics by changing the water depth felt by waves (Tolman, 1990; Wolf and Prandle, 1999; Pleskachevsky et al., 2009).

Many efforts have emphasized the significance of currents' effects on the waves, particularly under strong currents condition. In the southern North Sea, numerical investigation of Osuna and Monbaliu (2004) revealed that differences in significant wave heights (H_s) and mean periods due to currents could reach up to about 0.2 m and 1 s when currents speed up to 1 m/s. Following currents could reduce the wave height since the wave group propagates faster and therefore wave energy is dispersed (Fan et al., 2009); conversely, wave energy would be concentrated and H_s could be increased when waves encounter opposite currents (Warner et al., 2010). During a storm event, storm-driven strong currents could lead to the variations of H_s up to 0.6 m in the semi-enclosed Gulf of Venice (Benetazzo et al., 2013). In the tide dominated estuary investigated by Bolaños et al. (2014), wave period as well as H_s was modulated predominantly by the time-varying water depth, meanwhile, current-induced Doppler shift could exert a prime effect on wave period. Generally, taking currents' effects on waves into consideration could improve the performance of wave models, for instance, Guillou (2017) highlighted that introduction of tidal forcing into the wave model lead to ~30% variations of H_s by current-induced refraction, and therefore significantly improved the wave simulation; Rapizo et al. (2017) demonstrated that wave models tend to overestimate wave height on opposing currents, and introducing current-enhanced wave dissipation into the wave model considerably improved the simulation of wave height and mean wave period.

The Qiongzhou Strait (QS) is a 30-km wide tide-dominated busy shipping lane between the Leizhou Peninsula and the Hainan Island (Fig. 1), it is a key passage linking the Beibu Gulf and

Foundation item: The Fund of Southern Marine Science and Engineering Guangdong Laboratory (Zhanjiang) under contract No. ZJW-2019-08; the Program for Scientific Research Start-up Funds of Guangdong Ocean University under contract No. 101302/R18001; the National Natural Science Foundation of China under contract No. 41776034; the First-class Discipline Plan of Guangdong Province under contract No. CYL231419012.
*Corresponding author, E-mail: liucong175@gmail.com

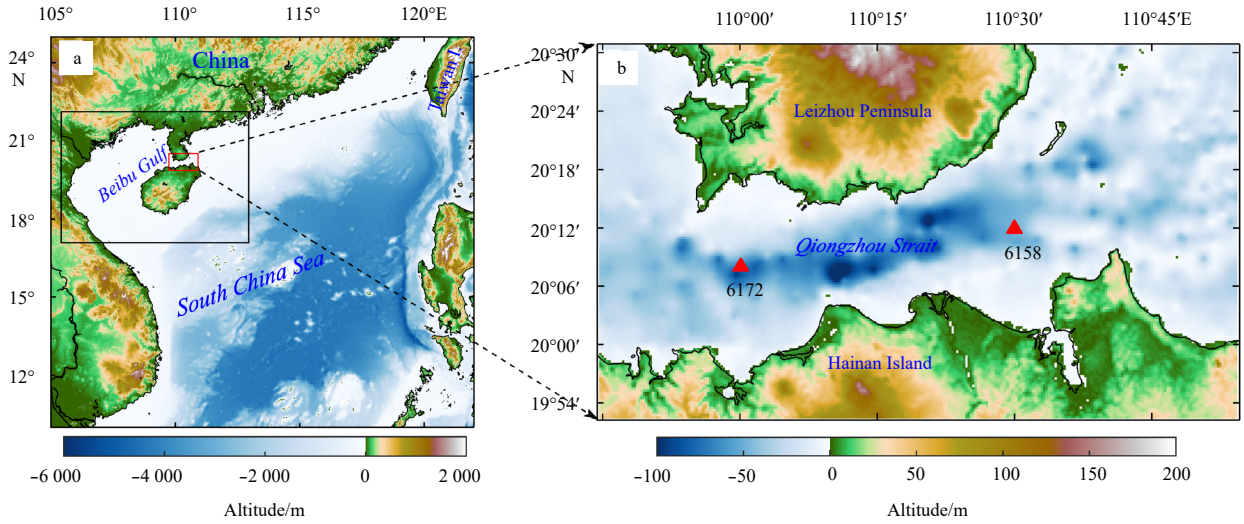

Fig. 1. Altitude of the study region (a) and magnified view of the child model domain (b). Black and red rectangles in a mark off the parent and child model domains, respectively; red triangles in b show the locations of Stas 6158 and 6172 of the China General Oceanographic Survey.

the Guangdong coastal seas with an averaged depth of 44 m, and the bathymetry can reach up to 120 m in the central strait. Tidal systems on both sides of the QS interact with each other through the strait, and the constriction effect of this narrow channel leads to intense tidal currents. In most areas of the QS, the maximum possible tidal current velocity could exceed 2.4 m/s (Wu et al., 2016). The semi-major axises of both the diurnal and semi-diurnal tidal currents are generally parallel to the QS as a consequence of the restriction by local topography (Shi et al., 2002; Chen et al., 2009; Zhu et al., 2014).

The prevailing southwest summer monsoon suffers the inhibiting effect of the Hainan Island, becoming weak and chaotic when it arrives the QS, and as a result, summer wind waves in the QS are mild and with chaotic wave directions. However, the strong northeast winter monsoon can blow directly over the QS, meanwhile, the waves in the open seas east to the QS can propagate into the strait straightforwardly, which thereby generates more powerful waves (~1 m high) in the QS.

The strong tidal currents in the QS provides a necessary condition for imposing significant modification on local wave dynamics, however, currently this topic has rarely been explored. To improve the understanding of currents' effects on waves in this strait, we had conducted a numerical investigation, in which we focused on the responses of winter waves to currents since winter waves are relatively more stable and stronger compared with other seasons. This study would contribute to local ocean navigation, engineering, hazard warning, and regulatory actions. The outline of the paper is as follows. Section 2 introduces the numerical model employed in this study, meanwhile, the model configurations and the numerical experimental design are also demonstrated; Section 3 presents the model results and discussion; Section 4 briefly summarizes the present work.

2 Model, modeling procedure, and numerical experiments

Currents' effects on the wave characteristics in the QS were numerically explored by taking advantage of the newly developed coupled ocean-atmosphere-wave-sediment transport (COAWST) modeling system (Warner et al., 2008, 2010). The COWST is a fully-coupled model which can accomplish the coupling of the Regional Ocean Modeling System circulation model (ROMS; Haidvogel et al., 2000; Shchepetkin and McWilliams, 2005), Weather Research and Forecasting atmosphere model (WRF; Skamarock et al., 2005) and Simulating WAves Nearshore wave model (SWAN; Booij et al., 1999). To simplify and focalize the discussion, only the circulation and wave modules were activated, and no waves' feedback was considered in the circulation module.

2.1 *ROMS circulation model*

The ROMS is a state-of-the-art regional ocean model, which solves the three-dimension Reynolds-averaged equations for conservation of mass, momentum, and heat. The ROMS configured for the present study was a barotropic tidal currents model, because tidal currents are dominant compared with components triggered by other forcing terms (e.g., stratification and air-sea fluxes) in the QS (Shi et al., 2002; Chen et al., 2009; Zhu et al., 2014). A two-layer nested model grid was designed to enhance the modeling resolution in the QS, the parent-grid extended from 17.10° to 22.12°N and 105.40° to 112.95°E (black rectangle in Fig. 1a), with a ~1.7 km horizontal resolution. Twenty levels of stretched terrain-following coordinate was applied in the vertical direction. The child-grid extended from 19.87° to 20.52°N and 109.74° to 110.91°E (red rectangle in Fig. 1a), with a ~347 m horizontal resolution, and vertically, twenty levels of stretched terrain-following coordinate was utilized. The topography was interpolated from a hybrid-data based on the GEBCO 30 arc-second product (https://www.bodc.ac.uk/) and the local sea chart. Vertical mixing coefficient was parameterized by the k-ε submodule of the Generic Length Scale (GLS) turbulence closure scheme (Umlauf and Burchard, 2003; Warner et al., 2005). Spatially uniform quadratic bottom friction ($C_d = 0.002\ 5$) was exerted at the bed. Tidal harmonic constants of ten tidal constituents (M_2, S_2, N_2, K_2, K_1, O_1, P_1, Q_1, M_f and M_m) interpolated from the TPXO7 data (http://volkov.oce.orst.edu/tides/) were added to the open boundaries of the parent-ROMS as tidal forcing. The time step was 300 s for the parent-ROMS and 60 s for the child-ROMS, and both with a model-splitting ratio of 30.

2.2 *SWAN spectral wave model*

The SWAN is a third-generation shallow water spectral wave model which could solve the wave generation, propagation, dissipation, refraction owing to currents and depth, and nonlinear wave-wave interactions. Within a Cartesian framework, the balance equation for the wave-action density spectrum $N(k,\theta)=F(k,\theta)/\sigma$ (F is the variance spectrum) can be written as:

$$\frac{\partial N}{\partial t}+\nabla\cdot(\dot{\boldsymbol{x}}N)+\frac{\partial}{\partial k}\left(\dot{k}N\right)+\frac{\partial}{\partial\theta}\left(\dot{\theta}N\right)=\frac{S_{\rm in}+S_{\rm nl}+S_{\rm ds}}{\sigma}, \quad (1)$$

$$\dot{\boldsymbol{x}}=\boldsymbol{c}_{\rm g}+\boldsymbol{U}, \quad (2)$$

$$\dot{k}=-\frac{\partial\sigma}{\partial D}\frac{\partial D}{\partial s}-\boldsymbol{k}\frac{\partial\boldsymbol{U}}{\partial s}, \quad (3)$$

$$\dot{\theta}=-\frac{1}{k}\left(\frac{\partial\sigma}{\partial D}\frac{\partial D}{\partial m}+\boldsymbol{k}\frac{\partial\boldsymbol{U}}{\partial m}\right), \quad (4)$$

where overdot indicates a derivative and bold letter indicates a vector, k is wavenumber, θ is wave direction, σ is the intrinsic frequency, $S_{\rm in}$ is the wind energy input, $S_{\rm nl}$ is the energy transfer due to nonlinear wave-wave interactions among spectral components, and $S_{\rm ds}$ is the wave decay through wave breaking ($S_{\rm ds,br}$), whitecapping ($S_{\rm ds,w}$), and bottom friction ($S_{\rm ds,b}$). $\boldsymbol{c}_{\rm g}$ is the group velocity, $\boldsymbol{U}$ is the ocean velocity vector, D is the water depth, s is a coordinate in the direction θ, $\boldsymbol{k}$ is the wavenumber vector, and m is a coordinate perpendicular to s. Further, by integrating the variance spectrum, the H_s can be derived as:

$$H_s=4\sqrt{E},\quad E=\iint F(k,\theta)\,{\rm d}k{\rm d}\sigma. \quad (5)$$

The SWAN model configured for the present investigation was also two-layer nested, which shared the same computational grids with the ROMS, respectively. Twenty-five frequencies ranging from 0.01 Hz to 1 Hz and thirty-six directional bands were used. Exponential wave growth based on Komen et al. (1984) and the Madsen bottom friction scheme were employed. We focused on the response of winter waves to the currents and to further simplify the discussion, the wave model was forced by spatially uniform wind with magnitude and direction being 5.4 m/s and 48.8°. Such wind forcing was based on the climatological winds (mean of January winds in 1979–2014) originated from the ERA-Interim database (http://apps.ecmwf.int/datasets/). The climatological H_s, mean wave period, and mean wave directions (mean of January waves in 1979–2014) interpolated from the ERA-interim database were added to the open boundaries of the parent-SWAN, meanwhile, the JONSWAP spectrum was utilized and a 20° directional standard deviation was used for directional spreading. The time step was 360 s for the parent-SWAN and 120 s for the child-SWAN, both layers generated an output every 1 hour.

2.3 *Modeling procedure*

The COAWST model is able to conduct online-nested wave-current coupling. However, to overcome the limitation of the computational capability, we first separately ran the online-nested ROMS and SWAN models for 40 d and gained the initial and boundary conditions for the child-ROMS and child-SWAN (first step), and then the child-ROMS and child-SWAN were coupled together (second step). During the first step, boundary forcings were exerted on the parent-ROMS and parent-SWAN open boundaries and both models were initialized with motionless state, the circulation model as well as the wave model could achieve a quasi-steady state after 30-d integration. In the second step, the initial field for the child-SWAN was generated based on the child-SWAN output of the 30th model day of the first step. Meanwhile, the boundary conditions could be obtained by using the child-SWAN outputs for the 30th–40th model days. Similarly, we generated the initial (output of the 30th model day) and boundary conditions (outputs of 30th–40th model days) for the child-ROMS. Finally, the child-ROMS and child-SWAN were coupled together and ran for 5 d to explore different currents' effects on waves. A flow chart describing the modeling procedures is presented in Fig. 2.

2.4 *Numerical experiments*

Both currents and free surface elevations play a vital role in modifying wave characteristics. In the COAWST model, these two effects could be considered by defining CURRENT and WLEV, respectively. We also defined UV_KIRBY scheme based on Kirby and Chen (1989) to account for the vertical structure of the velocity profile. To distinguish different roles played by currents and sea level variations in modifying the waves, four numerical experiments summarized as Table 1 were designed. In Table 1, Exps R1 and R2 are the child-ROMS and child-SWAN in the first step as presented in Fig. 2, respectively; Exp. R3 is the coupled child-

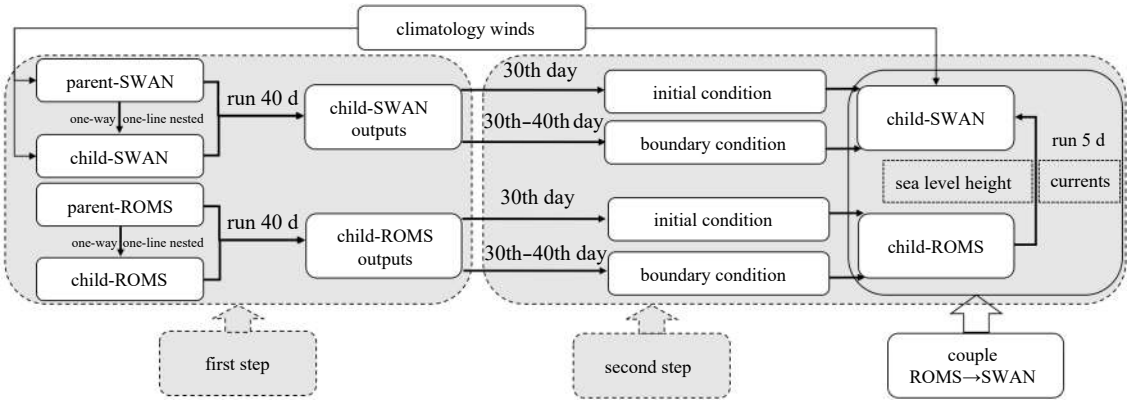

Fig. 2. Flow chart of the modeling procedure.

Table 1. Model configurations of all numerical experiments

	Experiment			
	R1	R2	R3	R4
Model	ROMS	SWAN	ROMS+SWAN	ROMS+SWAN
Currents' effects on waves	N/A	N/A	sea level variations	sea level variations and currents
Note	circulation-only case	wave-only case	partly-coupled case with sea level variations	fully-coupled case with both sea level variations and currents

SWAN-ROMS, which considers the influence of sea level variations on waves; Exp. R4 is the coupled child-SWAN-ROMS that allow both the currents and sea level variations to modify the waves. When coupled together, SWAN communicated with ROMS every 600 s.

3 Results and discussion

3.1 *Model validation*

The responses of waves to currents largely depend on the intensity of the tidal flow, thus, it is necessary to validate the model performance in simulating local tidal currents. The current profiles, observed at two 25-h stations in the QS (red triangles in Fig. 1b) during the China General Oceanographic Survey in February 1959, were used to validate the model results. As shown in Fig. 3, the child-ROMS provided reasonable simulations of the tidal currents in magnitude and direction at both eastern (Sta. 6158, Figs 3a and b) and western (Sta. 6172, Figs 3c and d) QS, the correlation coefficient and absolute mean error between the observed magnitudes and the modeled magnitudes were 0.74 m/s and 0.27 m/s, and 0.84° and 33.4° for flow directions, respectively. The child-ROMS omitted the non-tidal inflow, air-sea fluxes, and the stratification, which may account for the differences between the observations and simulations to a certain extent. Nevertheless, the comparisons indicate that the model could satisfactorily simulate the tidal currents in the QS.

Furthermore, we evaluated the model performance in wave simulation. Figures 4a and b present the H_s and peak wave direction based on the climatological ERA-Interim database and model results of the parent-SWAN, respectively. In the areas adjacent to the open boundaries of the parent-SWAN, the wave characteristics produced by the model agreed well with the ERA-Interim data (Figs 4a and b). In the central Beibu Gulf, the H_s was about 0.50–0.75 m during winter (Zong and Wu, 2014), however, the ERA-Interim product overestimated the H_s (>1.0 m) and produced wrong wave direction. This is mainly due to the low horizontal resolution of the ERA-Interim model, which fails to accurately describe the topography of the northwestern South China Sea and therefore underestimates the blocking effect of the Hainan Island and Leizhou Peninsula. Figure 4b reveals that results of our model were in good consistence with Zong and Wu (2014) and thus, our wave model could produce reasonable simulation of the waves in both the open and coastal seas.

3.2 *Winter wind waves in the QS*

Few previous investigations were dedicated to discuss wave characteristics in the QS. Teng and Wu (1993) investigated the wave dynamics in the QS based on wave observations at three stations. Their work revealed that wind waves were dominant in the QS and the major wave directions were NE-ENE. They also proposed that seasonal variations of the waves in the strait were significant. However, all the three stations were located in the

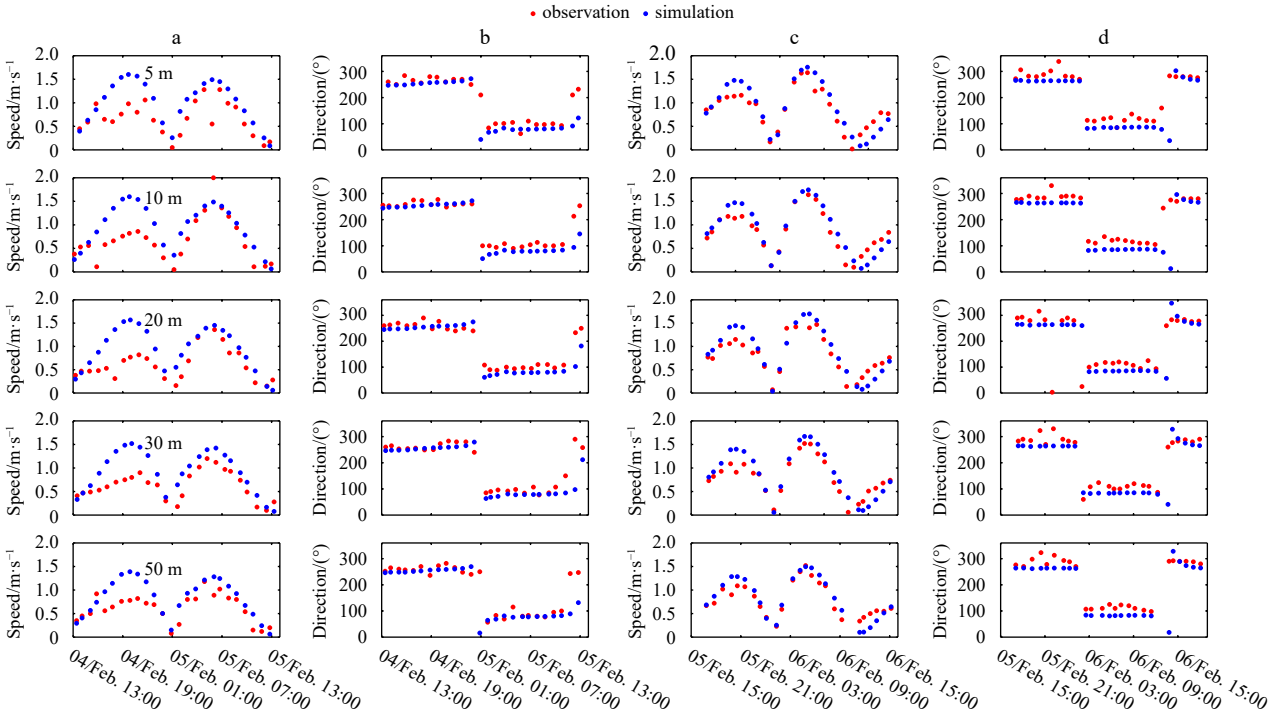

Fig. 3. Comparisons of the magnitude (column a) and direction (column b) at Sta. 6158, and the magnitude (column c) and direction (column d) at Sta. 6172 between the observed and the simulated tidal currents on 5 m, 10 m, 20 m, 30 m and 50 m layers, respectively.

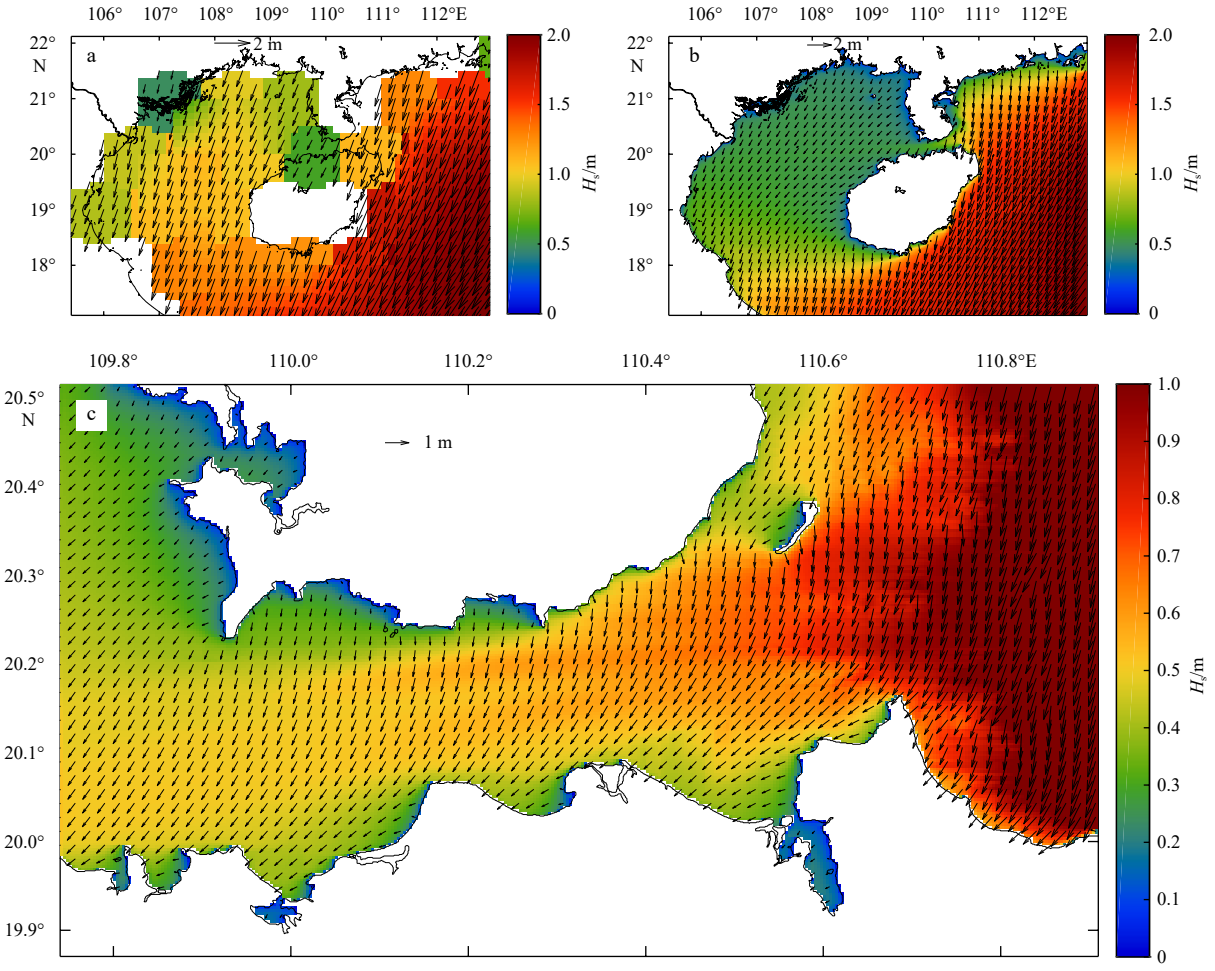

Fig. 4. Distributions of H_s (color-shading) and peak wave direction (arrows) over the northwestern South China Sea based on the climate-mean ERA-Interim database (a) and model results of the parent-SWAN (b), and the winter H_s and peak wave direction in the QS based on the model output of Exp. R2 (c).

nearshore areas shallower than 15 m and wave characteristics in the central strait were not discussed. The two-layer nested high-resolution SWAN model enables a global understanding of the waves in the strait.

Based on Exp. R2, Fig. 4c displays the H_s and peak wave direction in the QS during winter. When it came from east to west, the wave height gradually decreased and reached minimum in the west entrance (from 1.0 m to 0.5 m), indicating that the winter waves mainly propagate into the QS from the east entrance. Wave height in the central strait was larger than that in the nearshore areas, and presented a symmetric distribution along axial direction. Generally, the major wave direction in the QS was NE, which is consistent with Teng and Wu (1993).

3.3 *Influence of sea level variations*

Given the rule that stronger currents would trigger more significant adjustment of the waves (Phillips, 1977), the maximum eastward tidal currents (METC) and the maximum westward tidal currents (MWTC) were selected as two representative events for discussion. The tidal phases of the METC and the MWTC are displayed in Fig. 5a, and the surface horizontal velocity field and the sea level height filed of the METC and the MWTC are presented in Figs 5b and c, respectively. It should be noted that the wind-driven flow, tide-induced residual currents, and the density-driven currents contribute to a 5–40 cm/s westward surface mean flow in the QS in winter (Shi et al., 2002; Chen et al., 2009). Chen et al. (2009) demonstrated that the tide-induced westward residual flow is 10–20 cm/s in most areas of the QS. Therefore, the total contribution of wind-driven currents and density-driven currents may be estimated about 20 cm/s, which is important but is relatively small compared with the intense METC and MWTC (magnitude generally exceeds 1 m/s, Figs 5b and c), and thus neglecting wind forcing and stratification in the circulation model is generally acceptable.

The variations of sea level can change the total water depth felt by the waves, modifying the balance of the wave-action density spectrum, and thereby changing the H_s (Eqs (1)–(5)). Effect of sea level fluctuations on the H_s could be discussed by comparing the model results simulated by Exps R2 and R3, and the differences in H_s between these two experiments are shown in Fig. 6. We defined the region 19.87° to 20.52°N and 104.0° to 110.91°E as the east entrance area of the Qiongzhou Strait (EEAQS). Under the METC, the negative sea levels in the EEAQS (Fig. 6a) decreased the total water depth and exerted shoaling effect on the waves, and as a result, there were two patches located at the EEAQS where the H_s was increased by about 0.1 m (Fig. 6a). In these two patches, the bathymetry characterizes large spatial gradient, which will refract the wave rays and therefore concentrate the

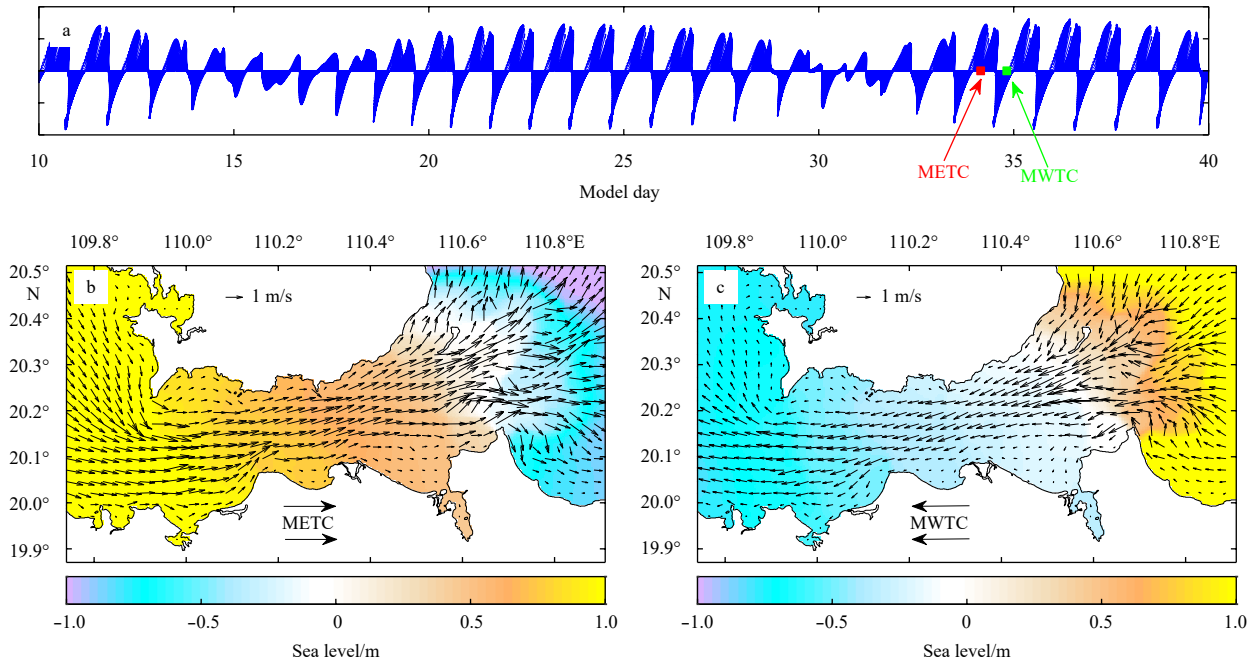

Fig. 5. Modeled time series of surface velocity vector at Sta. 6 158, tidal phases for the METC and the MWTC are marked as red and green squares, respectively (a); the surface horizontal velocity vectors superimposed on the sea level field under the METC (b) and the MWTC (c), respectively.

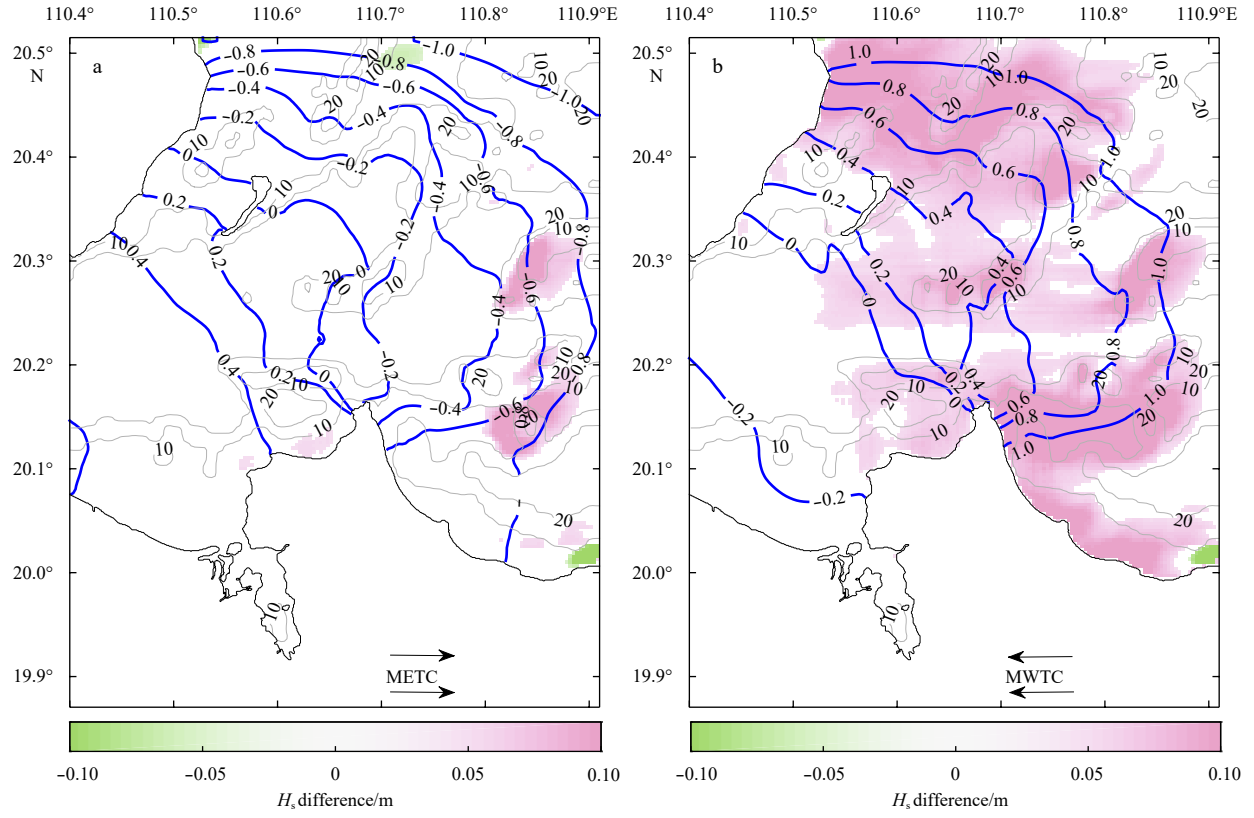

Fig. 6. Differences in the H_s (color shading, Exp. R3–Exp. R2) owing to the sea level variations under the METC (a) and the MWTC (b), blue contours indicate the sea levels, gray contours indicate the isobaths, differences in H_s below 0.05 m are not shown.

wave energy and contribute to higher wave height. Generally, the sea level variations under the METC only lead to minor adjustment over the whole QS (west part not shown). Under the MWTC, converse sea level pattern is presented as Fig. 6b, the positive sea level deepened the total water depth felt by waves, benefitting the westward propagation of the wave energy. Con-

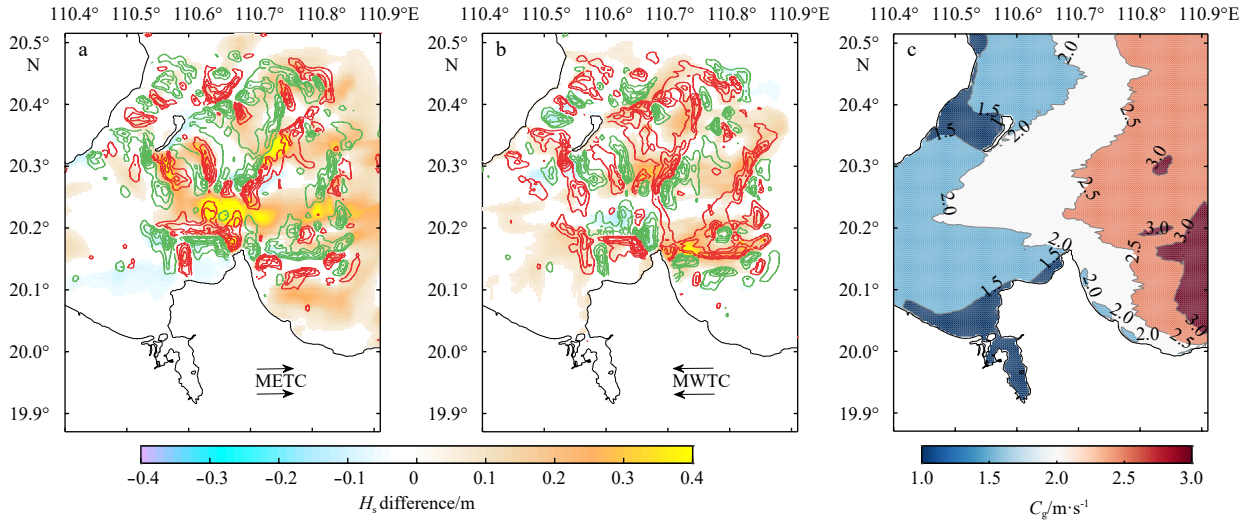

Fig. 7. Differences in the H_s (color shading, Exp. R4–Exp. R3) induced by the METC superposed by the divergence of the METC (red contours indicate convergence while green contours indicate divergence) (a); the same as a, but for the MWTC case (b); and distribution of wave group velocity originated from results of Exp. R2 (c). Note that differences in H_s below 0.05 m are not plotted.

sequently, higher wave height occurred in most areas of the EEAQS, and the enhancement of H_s by the MWTC was ~0.1 m. The QS is similar with the channel-shaped tidal estuary investigated by Bolaños et al. (2014), where the low tides restricted while high tides benefitted the further propagation of wave energy into the inner estuary.

3.4 *Influence of current-induced convergence*

As Eq. (2) reveals, the current-induced convergence can modify the H_s via modulating the propagation velocity of surface wave energy. When waves propagating into opposing currents, i.e., the METC, the tidal jet would concentrate the wave rays and focus wave energy, leading to larger wave height. Figure 7a shows the differences (Exp. R4–Exp. R3) in H_s due to the METC in the EEAQS, which reveals that the METC lead to a 20%–40% increase of the H_s.

To further interpret the model results, we performed analysis of unidirectional, monochromatic linear waves in condition of no wave generations and dissipations. For a deep-water wind wave (generally, $D>\lambda/2$ in the EEAQS) propagating from Area 1 with currents of magnitude U_1 to Area 2 with currents of magnitude U_2, the action fluxes satisfy:

$$\frac{E_1}{\sigma_1}\left(C_{g1}+U_1\right)=\frac{E_2}{\sigma_2}\left(C_{g2}+U_2\right). \tag{6}$$

Therefore, the change in H_s should be:

$$\frac{H_{s2}}{H_{s1}}=\sqrt{E_2/E_1}=\sqrt{\frac{\sigma_2}{\sigma_1}\frac{\left(C_{g1}+U_1\right)}{\left(C_{g2}+U_2\right)}}. \tag{7}$$

Equation (7) is identical to that derived by Longuet-Higgins and Stewart (1961) and utilized in Wang and Sheng (2018). Due to the current-induced wavenumber shift, the intrinsic frequency σ and group velocity $\boldsymbol{c}_g$ will change in Eq. (7), which will be discussed later. Here, we only consider the current-induced convergence effect, i.e., $\sigma_2=\sigma_1$ and $C_{g2}=C_{g1}$, then Eq. (7) is simplified into:

$$\frac{H_{s2}}{H_{s1}}=\sqrt{\frac{\left(C_{g1}+U_1\right)}{\left(C_{g1}+U_2\right)}}. \tag{8}$$

Considering a surface wave propagating into the QS with typical group velocity C_{g1} $\left(C_g=\frac{1}{2}\sqrt{g\lambda/2\pi}\right)$ being about 2.5 m/s (Fig. 7c). For the METC event (generally from still water to opposing currents), $U_1=0$ m/s and $U_2=-1$ m/s. Therefore, Eq. (8) estimates a 29% increase in the H_s, which is in good consistence with the information shown in Fig. 7a.

3.5 *Influence of current-induced wavenumber shift*

Differences in H_s triggered by the MWTC are presented as Fig. 7b, which indicates the wave height was generally increased by the following tidal currents. This is inconsistent with the above discussion in Section 3.4 (following currents will decrease the wave height). Moreover, Fig. 7a reveals that the current-induced convergence cannot explain several hot patches (marked with blue-dashed ellipses) where H_s increased by ~40%. Except for current-induced convergence, as Eq. (3) shows, the spatial gradients of currents in the travelling directions of the waves can lead to wavenumber shift. As a result, the change in $\dot{k}$ then leads to variations of $\boldsymbol{c}_g$ and σ, modifying the H_s in two ways (Ardhuin et al., 2017; Wang and Sheng, 2018): variations of σ can lead to exchange of energy between waves and currents; and the change of $\boldsymbol{c}_g$ can induce energy bunching and stretching. Due to the sharply varied topography in the EEAQS (Fig. 1b), the tidal flow there characterizes strong spatial gradient. Figure 7b reveals that the convergent areas of the MWTC are in good consistence with the locations where the H_s was increased, indicating current-induced wavenumber shift may play a significant role under the MWTC. Based on Eq. (7), change of the H_s induced by the wavenumber shift is:

$$\frac{H_{s2}}{H_{s1}}=\sqrt{E_2/E_1}=\sqrt{\frac{\sigma_{2C_{g1}}}{\sigma_{1C_{g2}}}}. \tag{9}$$

Given $C_g=\frac{1}{2}\frac{g}{\sigma}$, Eq. (9) equals to $H_{s2}/H_{s1}=\sigma_2/\sigma_1$. Based on the

conservation of the number of wave crests, Wang and Sheng (2018) proposed that the solution is $H_{s2}/H_{s1}=\sigma_2/\sigma_1=1+U_1/\left(2C_{g1}\right)$. Hence, under the MWTC (C_{g1}=2.5 m/s, $U_1=1$ m/s), the change of the H_s owing to wavenumber shift is estimated to be about 20%, which could explain most of the variations in the H_s shown in Fig. 7b. In addition, the two hot patches where H_s increased by about 40% in Fig. 7a may be a result of the joint effect by the wave-induced convergence and the wavenumber shift.

3.6 *Influence of current-induced refraction*

As Eq. (4) indicates, the gradients of currents along the wave crest direction ($\partial \boldsymbol{U}/\partial m$) can modify the wave direction, i.e., current-induced refraction. Also, Eq. (4) suggests this effect acts similarly as the variation of the topography ($\partial D/\partial m$). The differences in the peak wave direction caused by the METC are shown in Fig. 8a. Generally, the METC leads to counterclockwise rotation in peak wave direction in the northern part of the QS while clockwise rotation in the southern part. To simplify the discussion, Eq. (4) could be approximately written as $\dot{\theta}=-\dfrac{\boldsymbol{k}}{k}\dfrac{\partial \boldsymbol{U}}{\partial m}$. As shown in Fig. 5b, there was stronger tidal flow in the central strait while much weaker tidal currents in the northern and southern shoals, therefore, in the northern QS, $\partial\,|\boldsymbol{U}|/\partial m<0$, and in the southern QS, $\partial\,|\boldsymbol{U}|/\partial m>0$. Under the METC, the currents direction and the wave propagating direction were generally opposite with each other, i.e., $\boldsymbol{k}\cdot\boldsymbol{U}<0$. Thus, negative $\dot{\theta}$ in the northern QS while positive $\dot{\theta}$ in the southern QS could be inferred, which well explains the counterclockwise rotated peak wave directions in the northern QS (Figs 8a and c) and clockwise rotated ones in the southern QS (Figs 8a and d). Conversely, for the MWTC, the currents and waves generally propagated toward similar directions and therefore, $\boldsymbol{k}\cdot\boldsymbol{U}>0$, clockwise rotated peak wave directions would occur in the northern part of the QS (Figs 8b and e) while counterclockwise rotated peak wave directions occur in the southern part (Figs 8b and f). The magnitudes of the variations in peak wave direction reached up to 25°, indicating strong refraction by the currents. Moreover, the locations with the most significant variations in peak wave direction generally agreed well with the regions with sharp topography, which may indicate the extra contribution of the topography-induced refraction.

3.7 *Total effects of sea level variations and currents*

Figures 9a and b show the differences in H_s caused by the total effects of sea level variations and currents (Exp. R4–Exp. R2) under the METC and the MWTC, respectively. The total effects of the METC, also the MWTC, enhanced the H_s in the east entrance area of the Qiongzhou Strait, both with a spatially averaged increase of about 0.1 m. In several scattered patches (Figs 9a and b), changes in H_s triggered by the total effects of the METC and

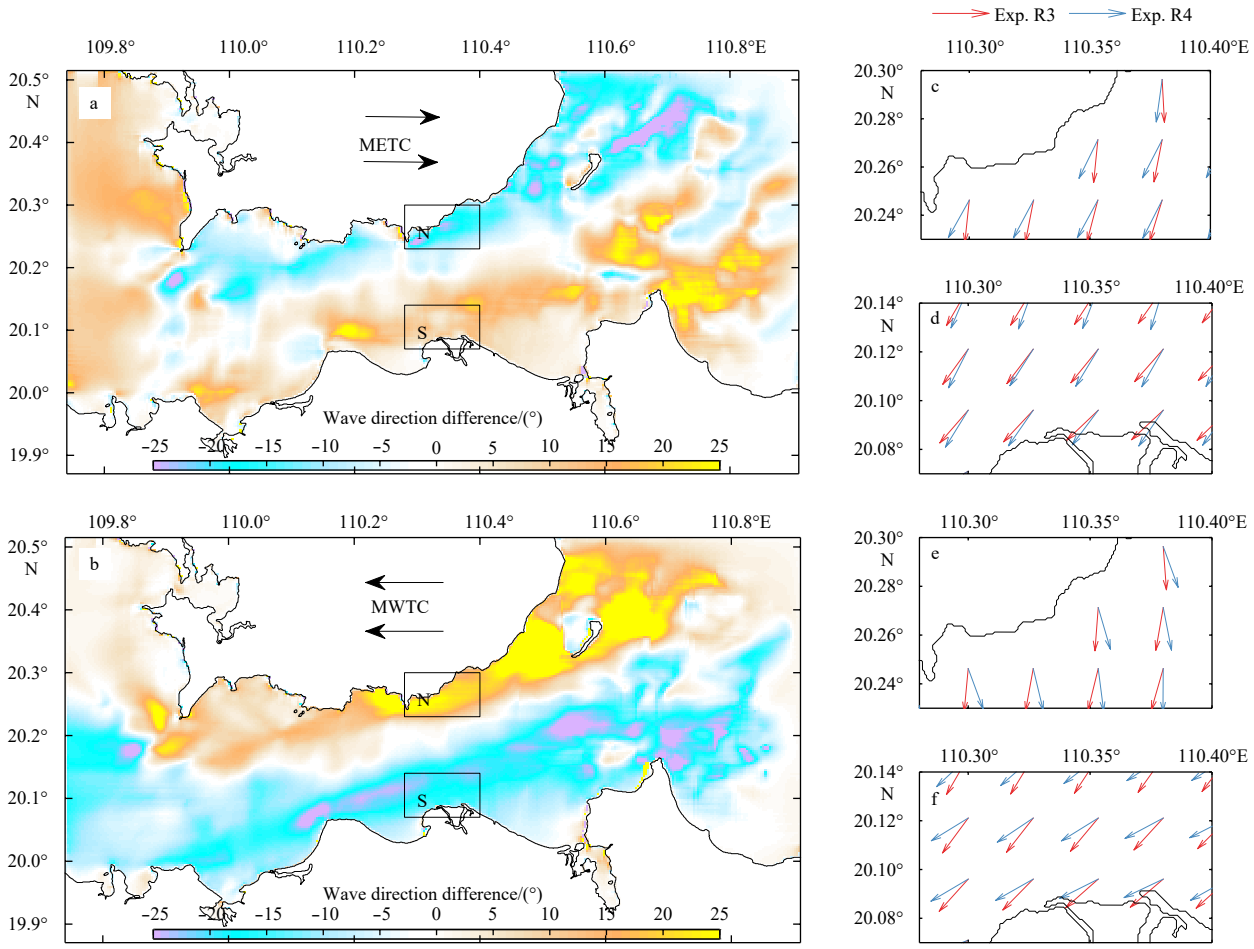

Fig. 8. Differences in peak wave directions (Exp. R4–Exp. R3) due to the METC (a) and due to the MWTC (b); the peak wave directions based on Exps R3 and R4 under the METC in Boxes N (c) and S (d) marked in a; and the peak wave directions based on Exps R3 and R4 under the MWTC in Boxes N (e) and S (f) marked in b.

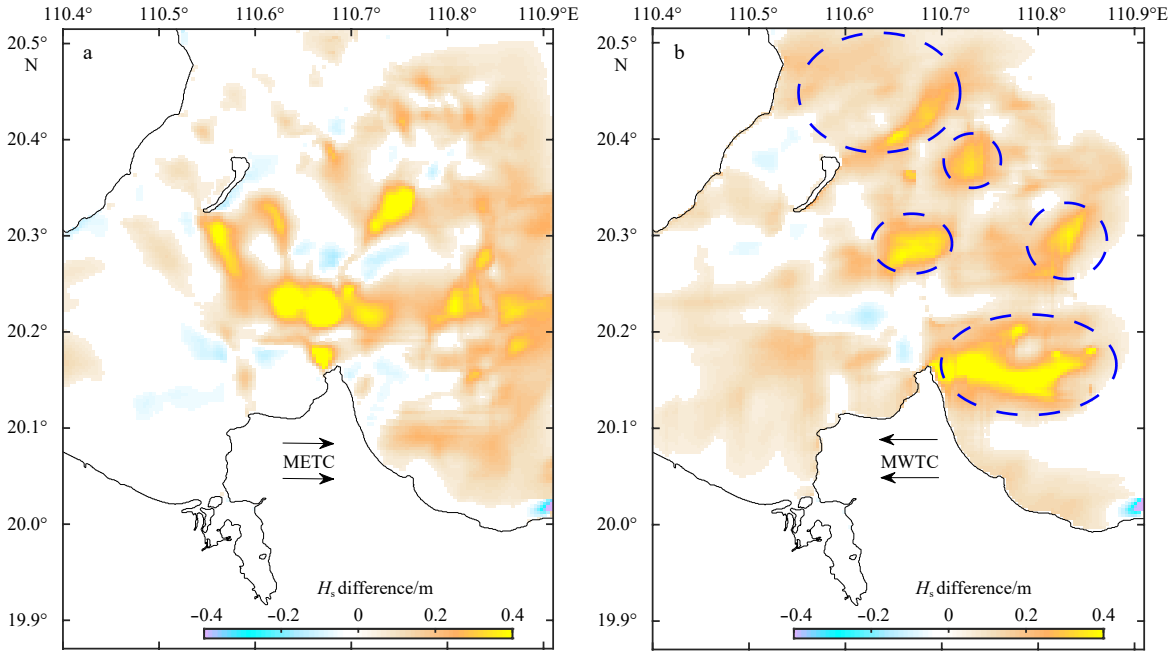

Fig. 9. Differences in the H_s (Exp. R4–Exp. R2) due to the total effects of sea level variations and currents under the METC (a) and the MWTC (b), differences in H_s below 0.05 m are not shown.

the MWTC could both exceed 40% (0.4 m), indicating the vital role of currents' effects in local wave dynamics.

Generally, differences in H_s shown in Figs 9a and b are very close to those displayed in Figs 7a and b, respectively, indicating a more significant contribution of currents than sea level variations. However, under the MWTC, significant differences between Figs 9b and 7b exist in the regions marked with blue-dashed ellipses (Fig. 9b). This is because, as discussed in Section 3.3, the positive sea level deepened the total water depth and benefitted the westward propagation of the wave energy, thereby leading to significantly enhanced H_s in these regions (~0.1 m, Fig. 6b).

4 Conclusions

Given that the strong tidal currents in the QS provides a necessary condition for imposing significant modification on strait wave dynamics, we have conducted a numerical investigation of currents' effects on winter wind waves in the QS by employing the COAWST modeling system. The model showed satisfactory performance in simulating the intense tidal currents in the QS when validated by observed current velocity data. Meanwhile, comparisons with former investigations revealed that the model could simulate reasonable wave dynamics in the studied area.

Three contrasted numerical experiments were designed to distinguish the different roles played by the sea level variations and the currents in modifying the waves. The METC and the MWTC were chosen as the two representative cases for showing how wave characteristics were modified by the currents because stronger currents lead to stronger adjustments in waves (Phillips, 1977). Model results showed that positive sea levels under the MWTC deepened the total water depth in the EEAQS, benefiting the further propagation of wave energy toward west and triggering increased wave height. The negative sea levels under the METC generally played a weak role in altering the wave height but could lead to significant enhancement of wave heights in several small shallow areas through shoaling effect.

Further discussions suggested that the current-induced convergence and wavenumber shift could exert significant influence on the waves, these two effects closely depend on the spatial gradients of currents (Wang and Sheng, 2018). Due to the sharply varied topography over the EEAQS, the tidal currents characterized strong spatial gradients (Shi et al., 2002; Chen et al., 2009) and therefore, waves there may experience the joint effect of current-induced convergence and wavenumber shift. Generally, effects of the METC-induced convergence and the MWTC-induced wavenumber shift could both increase the wave height in the EEAQS, and the former effect was more significant, which may because the METC-induced convergence can directly redistribute the wave energy (Eq. (2)). The METC and the MWTC can exert significant refraction on the waves, model results revealed that the METC (MWTC) lead to counterclockwise (clockwise) rotated peak wave direction in the northern part of the QS while clockwise (counterclockwise) ones in the southern part. Due to different physical mechanisms through which the METC and the MWTC modified the waves, the differences in H_s triggered by the METC and the MWTC were significantly different in spatial distribution, and the difference agreed well with satellite observed H_s.

By combining numerical simulation and theoretical analyses, the wave responses to the currents in the QS have been quantitatively explored, which emphasizes the significance of currents' effects on the winter wind waves in the QS. However, as previous studies demonstrated, the wave-enhanced bottom stress (Madsen, 1994), wave-mixing (Carniel et al., 2009; Wang et al., 2010; Li and Fox-Kemper, 2017), and the wave forces (Mellor, 2003; McWilliams et al., 2004) can play significant roles in modulating the currents, and thus modifying the waves, thereby resulting in feedback. Therefore, exploring the complete wave-current interaction in the QS would be an interesting future work. To simplify the study, climatological wave boundary conditions and spatially uniform winds were used to drive the model, and in the next stage, wave-current interaction modeling under realistic forcing

conditions is necessary to achieve further understanding of the hydrodynamics in the QS. Moreover, the scarcity of *in-situ* data on wave-current interaction (e.g., synchronous wave data, current velocity data, and sea level data) in the QS is another challenge and more targeted field observations are needed.

Acknowledgements

The first author sincerely thanks John C. Warner and Zengrui Rong for their generous and professional assistance in building up the COAWST model.

References

Ardhuin F, Gille S T, Menemenlis D, et al. 2017. Small-scale open ocean currents have large effects on wind wave heights. Journal of Geophysical Research: Oceans, 122(6): 4500–4517, doi: 10.1002/2016JC012413

Ardhuin F, Roland A, Dumas F, et al. 2012. Numerical wave modeling in conditions with strong currents: Dissipation, refraction, and relative wind. Journal of Physical Oceanography, 42(12): 2101–2120, doi: 10.1175/JPO-D-11-0220.1

Benetazzo A, Carniel S, Sclavo M, et al. 2013. Wave-current interaction: Effect on the wave field in a semi-enclosed basin. Ocean Modelling, 70: 152–165, doi: 10.1016/j.ocemod.2012.12.009

Bolaños R, Brown J M, Souza A J. 2014. Wave-current interactions in a tide dominated estuary. Continental Shelf Research, 109–123

Booij N, Ris R C, Holthuijsen L H. 1999. A third-generation wave model for coastal regions: 1. Model description and validation. Journal of Geophysical Research: Oceans, 104(C4): 7649–7666

Carniel S, Warner J C, Chiggiato J, et al. 2009. Investigating the impact of surface wave breaking on modeling the trajectories of drifters in the northern Adriatic Sea during a wind-storm event. Ocean Modelling, 30(2–3): 225–239, doi: 10.1016/j.ocemod.2009.07.001

Chen Changlin, Li Peiliang, Shi Maochong, et al. 2009. Numerical study of the tides and residual currents in the Qiongzhou Strait. Chinese Journal of Oceanology and Limnology, 27(4): 931, doi: 10.1007/s00343-009-9193-0

Fan Yalin, Ginis I, Hara T, et al. 2009. Numerical simulations and observations of surface wave fields under an extreme tropical cyclone. Journal of Physical Oceanography, 39(9): 2097–2116, doi: 10.1175/2009JPO4224.1

Guillou N. 2017. Modelling effects of tidal currents on waves at a tidal stream energy site. Renewable Energy, 114: 180–190, doi: 10.1016/j.renene.2016.12.031

Haidvogel D B, Arango H G, Hedstrom K, et al. 2000. Model evaluation experiments in the north atlantic basin: Simulations in nonlinear terrain-following coordinates. Dynamics of Atmospheres and Oceans, 32(3–4): 239–281, doi: 10.1016/S0377-0265(00)00049-X

Kirby J T, Chen T M. 1989. Surface waves on vertically sheared flows: approximate dispersion relations. Journal of Geophysical Research: Oceans, 94(C1): 1013–1027, doi: 10.1029/JC094iC01p01013

Komen G J, Hasselmann K, Hasselmann K. 1984. On the existence of a fully developed wind-sea spectrum. Journal of Physical Oceanography, 14(8): 1271–1285, doi: 10.1175/1520-0485(1984)014<1271:OTEOAF>2.0.CO;2

Li Qing, Fox-Kemper B. 2017. Assessing the effects of Langmuir turbulence on the entrainment buoyancy flux in the ocean surface boundary layer. Journal of Physical Oceanography, 47(12): 2863–2886, doi: 10.1175/JPO-D-17-0085.1

Longuet-Higgins M S, Stewart R W. 1961. The changes in amplitude of short gravity waves on steady non-uniform currents. Journal of Fluid Mechanics, 10(4): 529–549, doi: 10.1017/S0022112061000342

Madsen O S. 1994. Spectral wave-current bottom boundary layer flows. In: 24th International Conference on Coastal Engineering. Baltimore, MD: American Society of Civil Engineers, 384–398

Mellor G. 2003. The three-dimensional current and surface wave equations. Journal of Physical Oceanography, 33(9): 1978–1989, doi: 10.1175/1520-0485(2003)033<1978:TTCASW>2.0.CO;2

McWilliams J C, Restrepo J M, Lane E M. 2004. An asymptotic theory for the interaction of waves and currents in coastal waters. Journal of Fluid Mechanics, 511: 135–178, doi: 10.1017/S0022112004009358

Osuna P, Monbaliu J. 2004. Wave-current interaction in the Southern North Sea. Journal of Marine Systems, 52(1–4): 65–87, doi: 10.1016/j.jmarsys.2004.03.002

Phillips O M. 1977. The Dynamics of the Upper Ocean. 2nd ed. New York: Cambridge University Press

Pleskachevsky A, Eppel D P, Kapitza H. 2009. Interaction of waves, currents and tides, and wave-energy impact on the beach area of Sylt Island. Ocean Dynamics, 59(3): 451–461, doi: 10.1007/s10236-008-0174-1

Rapizo H, Babanin A V, Provis D, et al. 2017. Current-induced dissipation in spectral wave models. Journal of Geophysical Research: Oceans, 122(3): 2205–2225, doi: 10.1002/2016JC012367

Ris R C, Holthuijsen L H, Booij N. 1999. A third-generation wave model for coastal regions: 2. Verification. Journal of Geophysical Research: Oceans, 104(C4): 7667–7681, doi: 10.1029/1998JC900123

Shchepetkin A F, McWilliams J C. 2005. The regional oceanic modeling system (ROMS): a split-explicit, free-surface, topography-following-coordinate oceanic model. Ocean Modelling, 9(4): 347–404, doi: 10.1016/j.ocemod.2004.08.002

Shi Maochong, Chen Changsheng, Xu Qichun, et al. 2002. The role of Qiongzhou Strait in the seasonal variation of the South China Sea circulation. Journal of Physical Oceanography, 32(1): 103–121, doi: 10.1175/1520-0485(2002)032<0103:TROQSI>2.0.CO;2

Skamarock W C, Klemp J B, Dudhia J, et al. 2005. A Description of the Advanced Research WRF Version 2. Boulder, Colorado, USA: National Center for Atmospheric Research, NCAR/TN-468+STR

Teng Xuechun, Wu Xiujie. 1993. The wave characteristics in the Qiongzhou Channel. Journal of Oceanography of Huanghai & Bohai Seas (in Chinese), 11(4): 1–8

Tolman H L. 1990. The influence of unsteady depths and currents of tides on wind-wave propagation in shelf seas. Journal of Physical Oceanography, 20(8): 1166–1174, doi: 10.1175/1520-0485(1990)020<1166:TIOUDA>2.0.CO;2

Umlauf L, Burchard H. 2003. A generic length-scale equation for geophysical turbulence models. Journal of Marine Research, 61(2): 235–265, doi: 10.1357/002224003322005087

Vincent C E. 1979. The interaction of wind-generated sea waves with tidal currents. Journal of Physical Oceanography, 9(4): 748–755, doi: 10.1175/1520-0485(1979)009<0748:TIOWGS>2.0.CO;2

Wang Yonggang, Qiao Fangli, Fang Guohong, et al. 2010. Application of wave-induced vertical mixing to the K profile parameterization scheme. Journal of Geophysical Research: Oceans, 115(C9): C09014

Wang Pengcheng, Sheng Jinyu. 2018. Tidal modulation of surface gravity waves in the Gulf of Maine. Journal of Physical Oceanography, 48(10): 2305–2323, doi: 10.1175/JPO-D-17-0250.1

Warner J C, Armstrong B, He Ruoying, et al. 2010. Development of a coupled ocean-atmosphere-wave-sediment transport (COAWST) modeling system. Ocean Modelling, 35(3): 230–244, doi: 10.1016/j.ocemod.2010.07.010

Warner J C, Sherwood C R, Arango H G, et al. 2005. Performance of four turbulence closure models implemented using a generic length scale method. Ocean Modelling, 8(1–2): 81–113, doi: 10.1016/j.ocemod.2003.12.003

Warner J C, Sherwood C R, Signell R P, et al. 2008. Development of a three-dimensional, regional, coupled wave, current, and sediment-transport model. Computers & Geosciences, 34(10): 1284–1306

Wolf J, Prandle D. 1999. Some observations of wave-current interac-

tion. Coastal Engineering, 37(3–4): 471–485, doi: 10.1016/S0378-3839(99)00039-3

Wu He, Yu Huaming, Ding Jie, et al. 2016. Modeling assessment of tidal current energy in the Qiongzhou Strait, China. Acta Oceanologica Sinica, 35(1): 21–29, doi: 10.1007/s13131-016-0792-2

Zhu Xiaohua, Ma Yunlong, Guo Xinyu, et al. 2014. Tidal and residual currents in the Qiongzhou Strait estimated from shipboard ADCP data using a modified tidal harmonic analysis method. Journal of Geophysical Research: Oceans, 119(11): 8039–8060, doi: 10.1002/2014JC009855

Zong Fangyi, Wu Kejian. 2014. Research on distributions and variations of wave energy in South China Sea based on recent 20 years' wave simulation results using SWAN wave model. Transactions of Oceanology and Limnology (in Chinese), (3): 1–12